New Journal of Physics
The open-access journal for physics

Quantum simulator of an open quantum system using superconducting qubits: exciton transport in photosynthetic complexes

Sarah Mostame[1], Patrick Rebentrost[1], Alexander Eisfeld[1,2], Andrew J Kerman[3], Dimitris I Tsomokos[4] and Alán Aspuru-Guzik[1,5]

[1] Department of Chemistry and Chemical Biology, Harvard University, Cambridge, MA 02138, USA
[2] Max Planck Institute for the Physics of Complex Systems, Nöthnitzer Strasse 38, 01187 Dresden, Germany
[3] Lincoln Laboratory, Massachusetts Institute of Technology, Lexington, MA 02420, USA
[4] Department of Mathematics, Royal Holloway, University of London, Egham, TW20 0EX, UK
E-mail: aspuru@chemistry.harvard.edu

New Journal of Physics **14** (2012) 105013 (21pp)
Received 27 March 2012
Published 10 October 2012
Online at http://www.njp.org/
doi:10.1088/1367-2630/14/10/105013

Abstract. Open quantum system approaches are widely used in the description of physical, chemical and biological systems. A famous example is electronic excitation transfer in the initial stage of photosynthesis, where harvested energy is transferred with remarkably high efficiency to a reaction center. This transport is affected by the motion of a structured vibrational environment, which makes simulations on a classical computer very demanding. Here we propose an analog quantum simulator of complex open system dynamics with a precisely engineered quantum environment. Our setup is based on superconducting circuits, a well established technology. As an example, we demonstrate that it is feasible to simulate exciton transport in the Fenna–Matthews–Olson photosynthetic complex. Our approach allows for a controllable single-molecule simulation and the investigation of energy transfer pathways as well as non-Markovian noise-correlation effects.

[5] Author to whom any correspondence should be addressed.

Contents

1. Introduction **2**
2. The model Hamiltonian **3**
2.1. The system . . . 3
2.2. Coupling to the quantum environment . . . 4
2.3. The classical noise approximation . . . 5
3. The Fenna–Matthews–Olson (FMO) complex **6**
4. The simulator **7**
4.1. The system Hamiltonian . . . 7
4.2. Engineering classical noise . . . 8
4.3. Non-Markovian quantum approach . . . 10
5. Experimental feasibility **10**
6. Conclusion **13**
Acknowledgments **14**
Appendix A. Figures and tables **14**
Appendix B. Coordinate representation of the model Hamiltonian **17**
Appendix C. Energy transfer pathways for the FMO complex **18**
References **19**

1. Introduction

Understanding strongly interacting quantum systems with many degrees of freedom is one of the big challenges in physics and chemistry [1]. Classical computational methods are restricted by the exponentially increasing amount of resources required for the simulations. Quantum computers are conjectured to be a possible solution as the resources to simulate arbitrary quantum systems grow polynomially with the size of the system under study [2, 3]. However, universal quantum computers of sufficient size and performance are not available yet, one of the big problems being the loss of quantum mechanical coherence, i.e. decoherence [4]. Designing a special quantum system in the laboratory, which mimics the quantum dynamics of a particular model of interest, see for example, [5–10], can be a more viable alternative to an all-purpose quantum computer.

Here we propose a quantum simulator architecture using superconducting quantum bits (qubits) that is capable of simulating complex open quantum systems using currently available technology in realizable parameter ranges. We will focus on the Fenna–Matthews–Olson (FMO) pigment–protein complex on a single-molecule level. The recent observations [11, 12] of quantum beatings and long-lived quantum coherence in several photosynthetic light-harvesting complexes, such as the FMO complex in the green sulfur bacterium *Chlorobium tepidum* or the reaction center of the purple bacterium *Rhodobacter sphaeroides*, suggest possible evidence that quantum effects give rise to the high energy transport efficiency found for these complexes. There is a remarkable amount of recent theoretical research related to the question of the molecular structure, vibrational environment, origin and role of long-lived quantum coherences [13–23]. The electronic degrees of freedom are coupled to a finite temperature vibrational environment and the dynamics of the relevant electronic system

can be studied by means of open quantum system approaches. In quantum computing, the focus of much of the research has been on reducing the magnitude and influence of environmental decoherence and dissipation. However, controlled coupling to a dissipative environment can also be exploited [24–26]. In this work, we focus on *engineering* the decoherence to simulate open quantum systems that are challenging to study using classical computers.

We propose two approaches for simulating the vibrational environment. The first approach is based on engineering a classical noise source such that it represents the atomistic fluctuations of the protein environment. A prototypical experiment of environment-assisted quantum transport (ENAQT) can be performed [16]. The second approach allows for the precise engineering of the complex non-Markovian environment, i.e. an environment that has long-term memory. This is achieved by the explicit coupling of quantum inductor–resistor–capacitor (LRC) oscillators to the qubits which allows for energy and coherence exchange between the resonators and the qubits. Both approaches are based on present-day superconducting qubit implementations. We focus here on flux qubits, where two-qubit coupling was shown to be sign- and magnitude-tunable [27, 28] and methods of scaling to a moderate number of qubits have been discussed in [29]. We show that realistic simulation of photosynthetic energy transfer is feasible with current superconducting circuit devices.

2. The model Hamiltonian

We are interested in the dynamics of a finite dimensional system which is linearly coupled to a bath of harmonic oscillators. In the following we refer to the system as an 'electronic system' and to the quantum environment as a 'phonon bath' or 'vibrational environment'. The corresponding total Hamiltonian is written as

$$H_{\mathrm{tot}} = H_{\mathrm{el}} + H_{\mathrm{ph}} + H_{\mathrm{el-ph}}. \tag{1}$$

2.1. The system

We are often (e.g. in the FMO complex) interested in the transfer of a single electronic excitation. Thus basis states $|j\rangle$ are defined by the electronic excitation residing on molecule (site) j and all other sites being in their electronic ground state. The electronic Hamiltonian in this site basis is given by [30] $H_{\mathrm{el}} = \sum_{j=1}^{N} \tilde{\varepsilon}_j \, |j\rangle \langle j| + \sum_{i<j}^{N} V_{ij} \, (|i\rangle \langle j| + |j\rangle \langle i|)$.[6] The diagonal energies $\tilde{\varepsilon}_j$ are identified with the electronic transition energies of site j and the off-diagonal elements V_{ij} are the intermolecular (transition-dipole–dipole) couplings between sites i and j. Different local electrostatic fields of the protein at different sites shift the electronic transition energies [15], resulting in a complicated energy landscape.

[6] Here, $V_{ij} = \langle g_j \, e_i | \, V \, | g_i \, e_j \rangle$ with V being the electrostatic coupling between sites and $|g_i\rangle$, $|e_i\rangle$ denoting the electronic ground state and first excited state of site i, respectively. Note that $|i\rangle$ is defined throughout the paper by the electronic excitation residing on site i and all other sites being in their electronic ground state: $|i\rangle = |g_1 \, g_2 \, g_3 \cdots g_{i-1} \, e_i \, g_{i+1} \cdots g_N\rangle$.

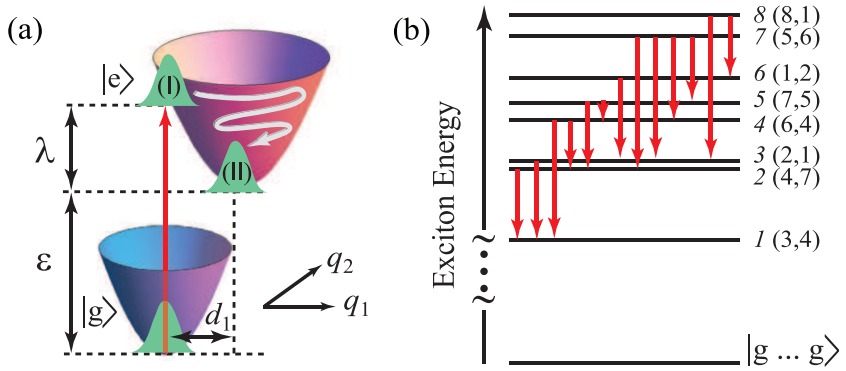

Figure 1. (a) Model of exciton-phonon dynamics in a system with two electronic states $|g\rangle$ and $|e\rangle$ and two dissipative vibrational modes q_1 and q_2. After a vertical Franck–Condon electronic excitation the phonon degrees of freedom are in a non-equilibrium position (I) from which the system relaxes to the displaced equilibrium configuration in the excited state (II). The displacements are given by d_1 and d_2 and the energy scale associated with this relaxation is the reorganization energy λ. This vibrational reorganization is not captured in most Markovian models. (b) Energy levels of the electronic Hamiltonian for the FMO complex denoted by $M(i, j)$, where (i, j) indicate the two most significant BChl pigments participating in the delocalized excitonic states M. The red arrows indicate the dominant pathways for the energy transport based on Redfield theory [17], see appendix C for more details.

2.2. *Coupling to the quantum environment*

The vibrational environment is represented by a set of displaced harmonic oscillators. The Hamiltonian of the phonon bath is written as $H_{\rm ph} = \sum_{j=1}^{N} H_{\rm ph}^{j}$, where $H_{\rm ph}^{j} = \sum_{\ell} \hbar\omega_{\ell}^{j}(a_{\ell}^{j\dagger} a_{\ell}^{j} + 1/2)$ with $a_{\ell}^{j\dagger}$ (a_{ℓ}^{j}) being the creation (annihilation) operator of excitations in the ℓth bath mode of site j. In the present work we restrict to the situation where each site has its own phonon environment which is uncorrelated with the phonon modes at the other sites. This is motivated by recent results obtained for the FMO complex [31, 32]. The diagonal part of the electronic Hamiltonian couples linearly to the phonon modes. The electron–phonon coupling term can be written as

$$H_{\rm el-ph} = \sum_{j=1}^{N} H_{\rm el-ph}^{j} = \sum_{j=1}^{N} |j\rangle\langle j| \left[\sum_{\ell} \chi_{j\ell} \left(a_{\ell}^{j\dagger} + a_{\ell}^{j} \right) \right]. \tag{2}$$

Here $\chi_{j\ell} = \hbar\omega_{\ell}^{j} d_{j\ell}$ is the coupling between the jth site and the ℓth phonon mode with ω_{ℓ}^{j} being the frequency of the ℓth phonon mode coupled to the jth site and $d_{j\ell}$ is the dimensionless displacement between the minima of the ground and excited state potentials of the ℓth phonon mode at site j. Notice that the so-called reorganization energy $\lambda_j \equiv \sum_{\ell} \hbar\omega_{\ell}^{j} d_{j\ell}^{2}/2$ was implicitly included in the above electronic transition energy $\tilde{\varepsilon}_j = \varepsilon_j + \lambda_j$ with ε_j being the energy difference between the minima of the potential energy surfaces for site j, see figure 1(a) and appendix B for more details.

It is known that complete information about the effect of the environment on a quantum system is determined by the spectral density (SD) function [34], which is defined by

$$J_j(\omega) = \sum_\ell |\chi_{j\ell}|^2 \delta(\omega - \omega_\ell^j), \tag{3}$$

for site j. Due to the high number of modes of the environment, $J_j(\omega)$ can be considered as a continuous function of ω. To account for finite temperature, we transform the SD [35, 36] $C_j(\omega, T) = \{1 + \coth[\hbar\omega/(2k_B T)]\}\, J_j^{\mathrm{A}}(\omega)$, where the subscript 'A' denotes the antisymmetric SD $J_j^{\mathrm{A}}(\omega) = J_j(\omega)$ if $\omega \geqslant 0$; and $J_j^{\mathrm{A}}(\omega) = -J_j(-\omega)$ if $\omega < 0$. The function $C_j(\omega, T)$ fulfills the detailed balance condition [35] and we name it 'temperature-dependent spectral density'.

It turns out that the relevant spectral densities of our problem can be approximated by a finite number of broadened peaks. These broadened peaks can often be associated with the vibrational modes of the molecules. Upon electronic excitation of a molecule, the vibrational wavepacket of the ground state is projected into a displaced wavepacket in the excited state, see figure 1(a). The wavepacket for the nuclei then moves on the excited state potential energy surface and dissipates energy (reorganizes) to the minimum energy point.

Finally, to facilitate the comparison with flux qubits we rewrite the total Hamiltonian (1) using Pauli matrices

$$\begin{aligned} H_{\mathrm{tot}} = {} & \frac{1}{2}\sum_{j=1}^{N} \tilde{\varepsilon}_j\, \sigma_z^j + \frac{1}{2}\sum_{i<j}^{N} V_{ij}(\sigma_x^i \sigma_x^j + \sigma_y^i \sigma_y^j) + \sum_{j=1}^{N}\sum_{\ell} \hbar\omega_\ell^j \left({a_\ell^j}^\dagger a_\ell^j + \frac{1}{2}\right) \\ & + \sum_{j=1}^{N}\sum_{\ell} \chi_{j\ell}\, \sigma_z^j ({a_\ell^j}^\dagger + a_\ell^j). \end{aligned} \tag{4}$$

Expressing the above Hamiltonian in the system energy eigenbasis, defined by $H_{\mathrm{el}}|M\rangle = E_M|M\rangle$, we have $H_{\mathrm{tot}} = \sum_M E_M |M\rangle\langle M| + \sum_{M,N,\ell} |M\rangle\langle N| \sum_j \mathscr{K}_{MN}^{j\ell}({a_\ell^j}^\dagger + a_\ell^j) + H_{\mathrm{ph}}$ with $\mathscr{K}_{MN}^{j\ell} = \langle M|j\rangle\langle J|N\rangle\, \chi_{j\ell}$. This shows that the system–bath coupling is off-diagonal in the eigenbasis.

2.3. The classical noise approximation

Although the main goal of the present paper is to simulate Hamiltonian (4) in a fully quantum mechanical fashion, it is also useful to consider the much simpler (but important) case where the quantum environment is replaced by time-dependent fluctuations of the transition energies. This is the basis of the often employed Haken–Strobl–Reineker (HSR) model for excitation transfer [37]. Furthermore, atomistic molecular dynamics using quantum mechanics embedded in molecular mechanics (MD/QM/MM) simulations [31–33] can readily provide noise time-series. In the classical noise approach, the system dynamics is obtained by averaging over many trajectories with the time-dependent Hamiltonian

$$\tilde{H}_{\mathrm{tot}} = \frac{1}{2}\sum_{j=1}^{N} \left[\tilde{\varepsilon}_j + \delta\tilde{\varepsilon}_j(t)\right] \sigma_z^j + \frac{1}{2}\sum_{i<j}^{N} V_{ij}(\sigma_x^i \sigma_x^j + \sigma_y^i \sigma_y^j), \tag{5}$$

where the influence of the environment is solely contained in the time-dependent site energy fluctuations $\delta\tilde{\varepsilon}_j(t)$. Often, as in the HSR model, it is assumed that the fluctuations are uncorrelated Gaussian white noise.

Table 1. Comparison of parameters for the FMO complex and the quantum simulator. The time scales shown below are for the dressed states of flux qubits coupled to the quantum harmonic oscillators. For more details see figure A.2 and tables A.1–A.3. Notice that the decay time in a single qubit ($\mathbb{T}_1$) does not need to be mapped directly from the FMO dynamics. With nowadays achievable decay times in superconducting qubits, which are three orders of magnitude larger than the excitation transfer time between the qubits, the dynamics of the FMO complex can be simulated.

Parameter	FMO model	Quantum simulator
Decay time ($\mathbb{T}_1$)	$\approx$ ns	$\approx 10\,\mu$s
Average exciton transfer time	≈ 5 ps	≈ 25 ns
Decay time between the exciton states	$\approx$ ps	≈ 5 ns
Dephasing in exciton manifold	≈ 100 fs	≈ 500 ps
Time scale of quantum beatings (τ_{osc})	≈ 200 fs	≈ 1 ns
Coupling between sites	≈ 10–$122\,\mathrm{cm}^{-1}$	≈ 60–730 MHz
Relative static site energy shifts	≈ 10–$500\,\mathrm{cm}^{-1}$	≈ 60 MHz–3 GHz
Temperature	300 K	60 mK

3. The Fenna–Matthews–Olson (FMO) complex

The model Hamiltonian (1) can be used to describe a single excitation in the FMO complex. The FMO complex acts as a highly efficient excitation wire, transferring the energy harvested by the photosynthetic antennae to a reaction center. The FMO complex has a trimeric structure exhibiting C_3-symmetry and each of the monomers consists of a network of eight [23] bacteriochlorophyll a (BChl a) pigment molecules. Since the coupling between monomers is very small and can be neglected on the time scales of interest, we focus on a single monomer in the following. The BChl pigments in the monomer are surrounded by a protein environment. Conformational motions of this protein environment (static disorder) are slow compared to the time scale of interest and affect energy levels of the pigments by electrostatic interaction [15]. The ranges of site energy differences $|\tilde{\varepsilon}_i - \tilde{\varepsilon}_j|$ and couplings V_{ij} are given in table 1. These parameters lead to the energy spectrum of the FMO monomer given in figure 1(b).

In the present work, we consider two spectral densities relevant to the FMO complex. Firstly, a model super-Ohmic SD [14], $J(\omega) = \lambda\,(\omega/\omega_{\mathrm{c}})^2\,\exp(-\omega/\omega_{\mathrm{c}})$ with reorganization energy $\lambda = 35\,\mathrm{cm}^{-1}$ and cutoff frequency $\omega_{\mathrm{c}} = 150\,\mathrm{cm}^{-1}$. We have dropped the subscript j under the assumption that all eight sites have same SD and reorganization energy. Secondly, the experimental SD [14, 38] discussed later in section 4.3. Notice that it is very challenging to simulate the experimental SD with current computational methods because of the apparent peaks and the mixing of vibrational dynamics caused by the electronic interaction between the sites. This structured SD with strong peaks is expected to lead to strong non-Markovian behavior.

In the biological situation, the FMO complex most likely obtains the excitation at sites 1, 6 or 8, since these BChls are close to the chlorosomal antennas, where photons are absorbed. It is often assumed that this excitation is initially local to these sites. Low energy site 3 is the target site for the excitation and is close to the reaction center where further biochemical processes

take place. In the ultrafast experiments, broad laser pulses excite a superposition of several delocalized exciton states.

4. The simulator

It is challenging to simulate the open quantum system described in the previous section on conventional computers [20, 36, 39], even using modern parallel processing units [40–42]. Here we propose using flux qubits coupled with tunable flux–flux couplings for this task. The environment is modeled by classical noise or quantum oscillators coupled to the flux qubits.

4.1. The system Hamiltonian

Consider first a single flux qubit. The relevant quantum states are the ones with magnetic flux pointing up $|\uparrow\rangle$ and down $|\downarrow\rangle$ or, equivalently, opposite directions of persistent current in the loop. In this bare basis, the Hamiltonian of a flux qubit is given by $H = (\varepsilon\sigma_z + \Delta\,\sigma_x)/2$, where ε is the energy bias between $|\uparrow\rangle$ and $|\downarrow\rangle$ and Δ is the tunnel splitting between the two states. Here $\varepsilon = 2I_p(\Phi_x - \Phi_0/2)$ [43] with I_p being the persistent current of the qubit and $\Phi_0 = h/2e$ being the flux quantum. We set $\varepsilon = 0$, since this is the case in most experiments (this is known as the optimal working point [43] since it reduces the qubits sensitivity to flux noise [44]).

A tunable transverse interaction between flux qubits equivalent to that in $H_{\rm el}$ can be realized using additional 'coupler' qubits [27, 45]. A schematic of such a simulator is given in figure 2(a). The Hamiltonian of the coupled qubit system can be written as $H_{\rm q} = \sum_{j=1}^{N} \Delta_j\,\sigma_x^j/2 + \sum_{i<j}^{N} g_{ij}(\Delta_{ij}^{\rm c})\,\sigma_z^i\,\sigma_z^j$ with $g_{ij}(\Delta_{ij}^{\rm c})$ being the coupling strength between flux qubits i and j, which is given by $g_{ij}(\Delta_{ij}^{\rm c}) \approx \mathcal{J}_{ij} - 2\,\mathcal{J}_{ic}\,\mathcal{J}_{jc}/\delta_{ij}$, where $\Delta_{ij}^{\rm c}$ is the (tunable) tunnel splitting of the coupler qubit and we have defined $\delta_{ij} \equiv \Delta_{ij}^{\rm c} - (\Delta_i + \Delta_j)/2$ and $\mathcal{J}_{mn} \equiv \mathcal{M}_{mn} I_p^m I_p^n$ with $m, n \in i, j, c$ [45]. Here, $\mathcal{M}_{mn}$ is the mutual inductance between qubits m and n. This expression is valid to leading order when $\delta_{ij} \gg |\Delta_i - \Delta_j|$, $\mathcal{J}_{ic}$, $\mathcal{J}_{jc}$. Notice that by choosing the magnitude of $\Delta_{ij}^{\rm c}$ to be smaller or larger than $(\Delta_i + \Delta_j)/2$ we can change the sign of the effective coupling. Rewriting the above Hamiltonian in the energy eigenbasis of the qubit $|\pm\rangle = (|\downarrow\rangle \pm |\uparrow\rangle)/\sqrt{2}$ converts $\sigma_x^j \to \sigma_z^j$ and $\sigma_z^i\,\sigma_z^j \to \sigma_x^i\,\sigma_x^j \approx \left(\sigma_x^i\sigma_x^j + \sigma_y^i\sigma_y^j\right)/2$ in the rotating wave approximation (neglecting strongly off-resonant couplings). This results in

$$H_{\rm q} \approx \frac{1}{2}\sum_{j=1}^{N} \Delta_j\,\sigma_z^j + \frac{1}{2}\sum_{i<j}^{N} g_{ij}(\Delta_{ij}^{\rm c})\,\left(\sigma_x^i\,\sigma_x^j + \sigma_y^i\,\sigma_y^j\right), \tag{6}$$

which is of exactly the same form as the system part (first line) of equation (4) with Δ_j and $g_{ij}(\Delta_{ij}^{\rm c})$ corresponding to $\tilde{\varepsilon}_j$ and V_{ij}, respectively. It is advantageous for the experimental implementation to note that the dynamics of equations (4) and (6) does not depend on absolute site energies $\tilde{\varepsilon}_j$ and Δ_j but only on energy differences $|\tilde{\varepsilon}_i - \tilde{\varepsilon}_j|$ and $|\Delta_i - \Delta_j|$, respectively.

The system of two coupled flux qubits shown in figure 2(a) can be extended to eight flux qubits with a special arrangement to simulate eight BChls. An experimental layout simulating the electronic part of the FMO Hamiltonian is given in figure 3, where Q_j represent flux qubits. Static disorder can be simulated in our proposed scheme by varying the tunnel splittings Δ_j in the flux qubits with each run of the experiment. First all the qubits are in the ground state by simply allowing the system to relax. Then they are initialized in a certain desired initial state to start the dynamics. The excitation of a qubit is straightforward to achieve with the application

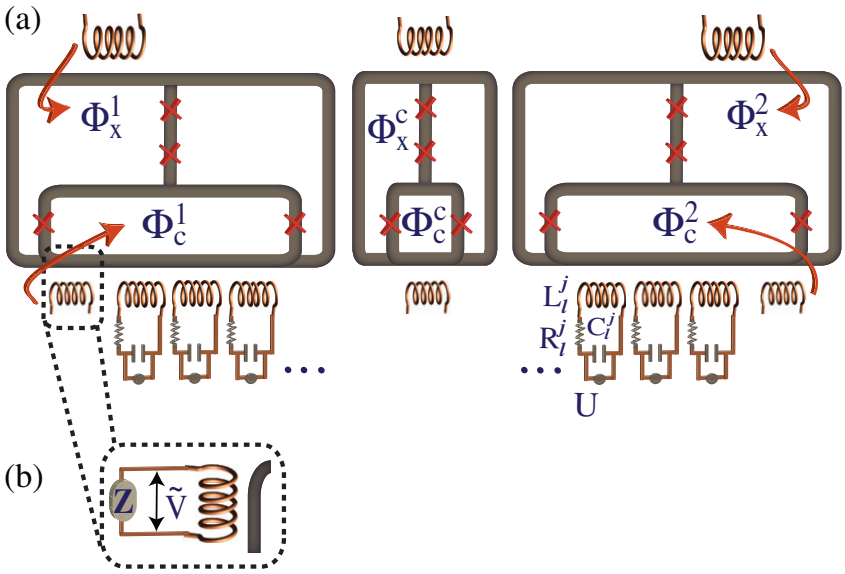

Figure 2. Circuit diagram of the proposed quantum simulator. (a) The qubit states are encoded in the quantized circulating current of the qubit loop. The red crosses denote Josephson junctions. Two flux qubits are coupled with a tunable $\sigma_z\sigma_z$-coupling. Each of the qubits is independently coupled to a finite number of quantum LRC oscillators to simulate the non-Markovian vibrational environment. The structure of the flux qubits are chosen to be gradiometric [46]. Coupling of the LRC oscillators to the smaller loop of the qubit leads to a diagonal coupling (σ_z-coupling), see section 4.3. With such a gradiometric structure, the magnetic fluxes due to the oscillators passing through the two parts of the larger loop are in different directions and cancel each other, and therefore, the off-diagonal coupling (σ_x-coupling), given by coupling of the oscillators to the larger loop of the qubit, is nearly zero. (b) Simulating the vibrational environment by adding a classical noise to each qubit.

of a resonant microwave excitation (π-pulse) carried by a microwave line which is connected to the respective qubit [43, 47]. After some evolution time the populations of the $|\pm\rangle$ states of the qubits are measured. The measurement is initiated by applying a flux pulse to shift the qubit away from $\mathscr{E} = 0$ so that its eigenstates become largely $|\uparrow\rangle$ and $|\downarrow\rangle$ which can be distinguished via the flux induced in a nearby dc superconducting quantum interference device (SQUID) loop. This pulse should be adiabatic with respect to the qubit's tunnel splitting (Δ) but fast compared to its couplings to other qubits. In addition, to capture the effect of reaction centers on the dynamics, we propose to add excitation sinks into the superconducting circuit, see figure 3. This is done with additional terminated transmission lines or shunt resistors coupled to those sites that are supposed to leak excitations.

4.2. Engineering classical noise

We will first discuss the more simple case of an environment treated within the classical noise formalism of equation (5). The basic idea of this approach is to simulate the fluctuations of the transition energies by coupling classical noise to the qubits via the flux Φ_c^j, see figure 2(b).

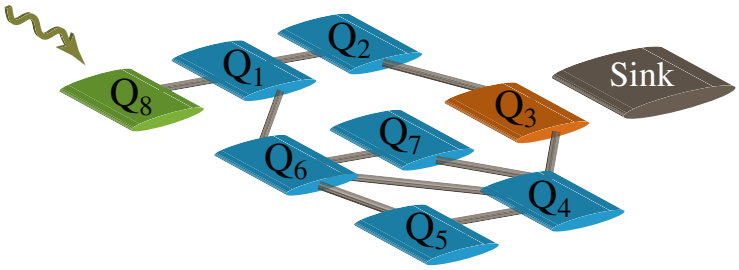

Figure 3. Experimental layout for simulating the exciton dynamics and ENAQT in the FMO complex (the architecture is based on the interactions given in [23], where for simplicity of the graphic the couplings below 15 cm^{-1} are not shown). Q_i represent single flux qubits. To simulate a biologically relevant case, one of these qubits, Q_8 shown in green, is prepared initially in the excited state while the others are set to the ground state. The measurement is performed on the target site, Q_3 shown in red. Sinks can be used to trap the energy and quantify the transfer efficiency.

Such a noise affects the tunnel splitting Δ_j in the qubit Hamiltonian. The noise can be actively created and sent to the qubit by a time-dependent voltage $\tilde{V}$ applied to a control loop [48].

With simple classical noise a prototypical experiment of ENAQT can be performed [16], see figure 3. Here we briefly discuss the main features of ENAQT and what is to be expected from an experiment scanning the ratio of dephasing rate over system energy scale. For the qubit system in our proposed quantum simulator, the couplings and the differences in the qubit splittings give a general energy scale Λ. The site energy level fluctuations lead to pure dephasing as the dominant decoherence mechanism, which is phenomenologically characterized by a pure dephasing rate γ. Each site can be driven, for example, by white noise with an (adjustable) amplitude $\sqrt{\gamma}$. If the dephasing rate γ is much smaller than the energy scale Λ, quantum localization is predicted to arise from the disorder in the energy levels. This leads to a small population at the target site. Increasing the dephasing rate such that $\gamma \approx \Lambda$ is expected [16] to lead to an increased population at the target site. Finally, it is expected that for the dephasing rate $\gamma \gg \Lambda$ diminished population arrives at the target site, since quantum transport is suppressed by the Zeno effect. In the FMO complex, the initial state of the simulation can be a single site excited (either site Q_1, Q_6 or Q_8 which are close to the antenna in the biological system). Measurement of success of the transport is performed at site Q_3, where the outcome is the population (zero or one) of the target site in the energy eigenbasis of the qubit. Performing the measurements at various times provides a trajectory of the site population. To simulate static disorder, such single trajectory measurements are performed for many different tunnel splittings Δ_j. The average then gives the ensemble value of the target population, which quantifies the efficiency.

Such an experiment can show that the environment is not always adversarial, but instead can make certain processes, like quantum transport, more efficient. This transport efficiency should exhibit a maximum at a dephasing rate that corresponds to room temperature in the biological system [16]. Similar ideas for simulating ENAQT based on coupled semiconductor quantum dots and quantum-optical cavities have been pursued in [49–51].

4.3. Non-Markovian quantum approach

In order to simulate the complex environment described by equation (4) and capture the non-Markovian effects, we propose to couple each of the flux qubits inductively to an independent set of a few damped quantum LRC oscillators, see figure 2(a). The coupling Hamiltonian between the qubits and oscillators [52] in the uncoupled qubit energy eigenbasis is given by $H_{\mathrm{q-osc}} = \sum_{j=1}^{N_{\mathrm{LRC}}} \sum_k \eta_{jk}\, \sigma_z^j (b_k^{j\dagger} + b_k^j)$ with $b_k^{j\dagger}$ (b_k^j) being the creation (annihilation) operator of the kth oscillator in site j and N_{LRC} denoting the number of LRC oscillators coupled to a single qubit. The coupling strength is given by $\eta_{jk} \equiv \mathscr{M}_{jk}\, I_0^{jk}\, \mathscr{R}_j$, where $I_0^{jk} = \sqrt{h\mu_0^{jk}/L_{jk}}$ is the root mean square (RMS) amplitude of the current in the kth oscillator ground state with μ_0^{jk} being the transition frequency of the oscillator and L_{jk} being the inductance of the oscillator. The parameter $\mathscr{R}_j = \mathrm{d}\Delta_j/\mathrm{d}\Phi_{\mathrm{c}}^j$ is the sensitivity of the qubit splitting to flux.

To simulate the original SD given by equation (3), we have to design the frequencies and couplings of the oscillators in such a way that the SD is reproduced up to a global scaling factor. Note that the temperature mapping is discussed in the next section. From the implementation point of view, we are limited to a finite number of oscillators. Thus we decompose the SD of interest into a moderate number of spectral densities of damped oscillators. The SD of a single oscillator coupled to a flux qubit can be derived by using a quantum Langevin equation approach [53, 54] and following the detailed balance condition [35]

$$C_{\mathrm{osc}}(\omega, T) = \mathfrak{D}\left[\frac{\mathrm{e}^{\hbar\omega/k_{\mathrm{B}}T}}{\kappa^2 + 4(\omega - 2\pi\mu_0)^2} + \frac{1}{\kappa^2 + 4(\omega + 2\pi\mu_0)^2}\right], \tag{7}$$

where $\mathfrak{D} = (\sqrt{8/\pi}\,\kappa\eta^2)/(\mathrm{e}^{h\mu_0/k_{\mathrm{B}}T} + 1)$ with η being the coupling strength of the oscillator to the flux qubit. Here, $\kappa = \kappa_0 \exp(-|\omega|/\alpha)\, \omega^2/\mu_0^2$ with κ_0 being the damping rate and α being a free parameter chosen reasonably to get the desired SD. By knowing the above SD for the damped quantum oscillators, we first simulate the temperature-dependent super-Ohmic SD. At 300 K this SD can be simulated with a set of six LRC oscillators coupled to each of the flux qubits, see figure 4(a), and at 77 K it can be simulated with a set of seven oscillators, see figure A.1(a). For the experimental SD, we need to couple, for example, 15 oscillators to each qubit, see figure 4(b). Notice that the so-obtained SDs in figure 4 are highly accurate and we can use fewer coupled oscillators if we are interested in less details of the spectral densities. The coupling of the oscillators to the flux qubit results in an additional shift of the qubit tunnel splitting Δ_j due to the reorganization energy of the oscillators. This has to be taken into account in the design of the energy landscape of the superconducting circuit.

5. Experimental feasibility

The simulation of the time evolution of the FMO complex requires a moderately coherent eight-qubit system, which would be realizable using the flux qubits demonstrated in [46]. In the FMO complex the site energies (chlorophyll excitation energies) are around 12 500 cm^{-1}, with the average site-dependent static shifts of the order of 250 cm^{-1}. We emphasize again that only the *site energy differences*, not the site energies themselves, play a role in the single exciton dynamics. The magnitudes of the coupling strengths between the chlorophyll molecules are smaller than 120 cm^{-1} [14]. For superconducting flux qubits, implementable range of the tunnel bias Δ_j is in the range of approximately zero to 13 GHz [46], while the coupling strengths g_{ij}

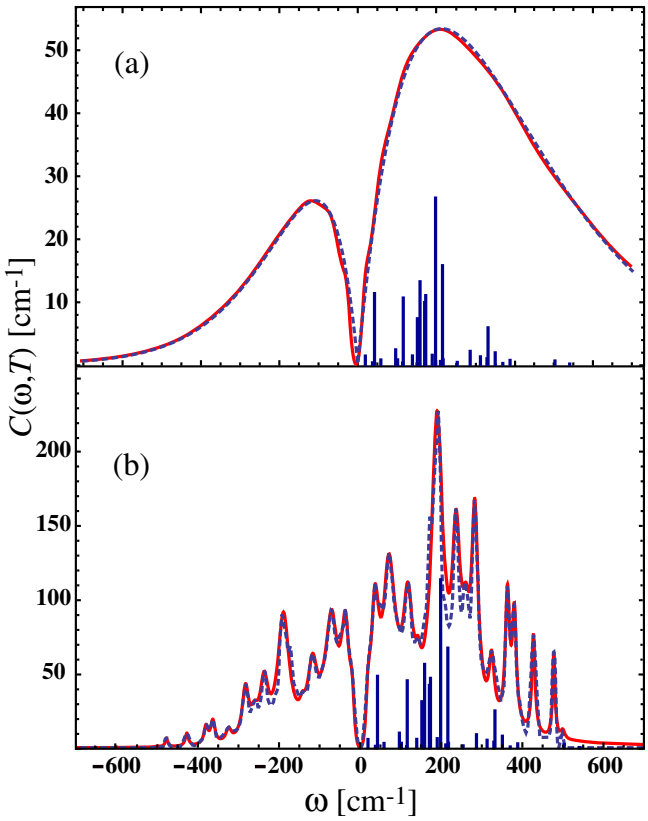

Figure 4. The parameterization of the temperature-dependent (a) super-Ohmic SD and (b) experimental [38] SD of the FMO complex into distinct quantum oscillators. The blue dashed lines are the spectral densities and the red solid lines are highly accurate simulation with LRC oscillators coupled to the flux qubits, see figure 2(a). The temperature for both spectral densities is 300 K. The super-Ohmic SD is simulated with six damped LRC oscillators and the experimental one is simulated with 15 damped oscillators. The blue bars show the transition energies [14] for the FMO complex. The obtained parameters are given in tables A.2 and A.3.

were measured up to 1 GHz [27]. In the proposed quantum simulator, the only restriction on Δ_j is that to be larger than any of the $|\Delta_i - \Delta_j|$ and any of the g_{ij}. Since these parameters are all smaller than 3 GHz, Δ_j can be chosen to be around 5–10 GHz, which is very reasonable for flux qubits. As has been mentioned above, the Δ_j are not physically important in the single exciton dynamics and it is the differences $|\Delta_i - \Delta_j|$ which play a role. Therefore, Δ_j could also be larger if the qubits are capable of it.

The parameters of the proposed quantum simulator are scaled through the time scale of quantum beatings ($\tau_{\rm osc}$) to be consistent internally as well as with the implementation restrictions, see table 1. Photosynthesis occurs at ambient temperatures, e.g. 300 K, which then maps to 60 mK in our proposed superconducting-circuit experiments. The FMO dynamics is usually considered for up to 5 ps, which translates to the time scale of 25 ns in the flux qubits. The energy relaxation time ($\mathbb{T}_1$) of a single qubit has been found [47, 55] to be on the order of a few μs, being a few orders of magnitude larger than the required exciton transfer time. Several

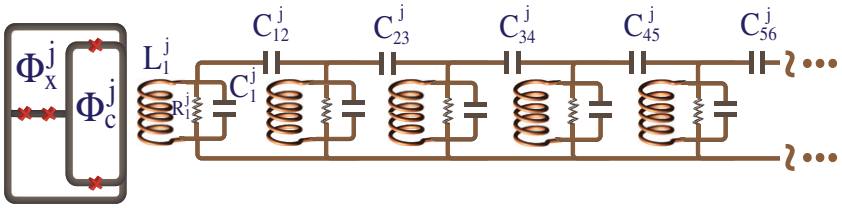

Figure 5. The parallel combination of LRC oscillators shown in figure 2(a) can be mapped to a linear chain of oscillators, such that only a single resonator would need to be coupled directly to each qubit. The oscillators can be coupled, for example, capacitively via capacitors C_{mn}^j.

coherent beatings between two coupled qubits have been observed [27]. Table 1 represents the summary of the proposed range of parameters for the superconducting simulator to imitate the dynamics of the FMO complex.

In simulating the quantum environment of the FMO complex, the required transition frequency of the LRC oscillators are in the range of 120 MHz–3 GHz and the coupling to the qubits are around 8–100 MHz, see tables A.2 and A.3. These parameters are experimentally reasonable. Although the geometry of figure 3 can provide coupling of an oscillator purely to the qubit's Φ_c (and NOT Φ_x) if that oscillator shares the qubit's symmetry axis, this symmetry cannot be maintained if many oscillators are required. To circumvent this problem, the parallel combination of resonators used to implement the desired SD can be mapped, for example, to a linear chain of oscillators [56–58], such that only a single resonator would need to be coupled directly to each qubit, see figure 5. This chain configuration will also make it easier to geometrically fit several oscillators coupled to each qubit without spurious parasitic couplings. The quality factor (transition frequencies/bandwidth) of the quantum oscillators in our proposed simulator are 50 or less. The coupling to the output line can be tunable to adjust the quality factor of each oscillator *in situ*. In [46], values of the flux sensitivity of the gap $\mathscr{R}_j$ up to $0.7\,\mathrm{GHz/m}\Phi_0$ were demonstrated. However, this quantity should be kept as small as possible to reduce coupling of flux noise to the qubit splittings. We therefore seek to maximize the other factors in the coupling. To do this, we first take a relatively large mutual inductance of $\mathscr{M}_{jk} = 10\,\mathrm{pH}$ between the oscillator and the qubit control loop. This value is bounded by: (i) it must be kept much smaller than the Josephson inductance of the two small junctions in the dc SQUID to avoid significant perturbations of the qubit itself; and (ii) much larger than this would require multiple windings or wiring layers, given the physical size of the loops concerned. With $\mathscr{M}_{jk}$ fixed, the coupling strength is then maximized by minimizing the oscillators' inductance. We choose a value of $L_{jk} = 100\,\mathrm{pH}$, such that $\mathscr{M}_{jk} = 10\,\mathrm{pH}$ does not significantly renormalize the oscillator frequency (as would be the case if L_{jk} and $\mathscr{M}_{jk}$ were comparable). Then, for an oscillator frequency of 120 MHz we require $C_{jk} = 10\,\mathrm{nF}$. This is quite large, but achievable in a parallel-plate geometry using sizes of the order of a few 100 μm. These parameters give a maximum coupling strength of 95 MHz, about five times larger than the required 18 MHz. Thus, we can then reduce $\mathscr{R}_j$ by a factor of five to achieve the desired coupling. For an oscillator of 1.1 GHz, we require $C_{jk} = 300\,\mathrm{pF}$, which gives a maximum coupling of 290 MHz, about three times larger than the required 99 MHz. These examples show that the parameters given in tables A.2 and A.3 are plausible. Note that the quality factor of these resonators is extremely low, so that standard fabrication techniques can be used.

Implementation of our proposed simulator will be a challenging task, requiring a larger collection of qubits (18) than have yet been demonstrated (currently up to four qubits have been

observed in a single circuit [59, 60]). Additional engineering complications may arise beyond those that have previously been addressed in single- and few-qubit experiments. For example, cross talk between control lines can already be a challenging problem even in few-qubit systems. In our case, this problem is mitigated by the fact that in the simplest scheme the many bias lines are only used for static (rather than dynamic) control; therefore even if there are cross-couplings, these can be diagonalized out to obtain the combination of physical bias adjustments necessary to tune each individual Hamiltonian parameter. Another type of parasitic would be cross-coupling between one set of oscillators and the qubit corresponding to another set. This would create correlations between the environments seen by each qubit which go beyond the model we are simulating. Another concern might be that coupling of each qubit to many oscillators might provide additional, spurious dissipation channels which could significantly reduce the lifetime of the individual qubits. Of course this cannot be ruled out without doing an actual experiment; however, one favorable aspect of the proposed system in this regard is that the coupling of the oscillators to the (bare) qubits is in principle purely longitudinal, i.e. the (bare) qubits cannot exchange photons with the oscillators and therefore cannot relax due to an interaction with them [61, 62]. This fact relies on the gradiometric geometry of the qubits (figure 2), and the chain model for the oscillators (figure 5), which exploits the qubits' geometric symmetry to suppress spurious transverse coupling. It is important, however, to emphasize the fact, illustrated in figures 1(b) and A.2(c), that once the qubits are coupled to each other, the coupling of the collective modes of the system to the oscillators becomes transverse, such that photons can be exchanged between the oscillators and the collective modes of the system. This is precisely what we propose to emulate. All of the above numbers and observations suggest that the site energy differences to coupling ratios of the FMO complex as well as corresponding temperature and environmental couplings are achievable with superconducting circuits.

6. Conclusion

We have demonstrated that an appropriately designed network of superconducting qubit-resonator design can simulate not only the coherent exciton transport in photosynthetic complexes, but also the effect of a complicated quantum environment. We have highlighted its experimental feasibility with present-day technology. In particular, we have shown that a straightforward combination of superconducting qubits (representing the chlorophyll molecules) and resonators (simulating the phonon environment) can be used to obtain a reasonable approximation to the exciton and phonon degrees of freedom in the FMO complex. For example, we show ways to engineer an SD that reproduces that of a biological system. One of the advantages of our proposed quantum simulator, compared to the computational methods, is simulating both diagonal and off-diagonal noise. Because of the additional complexity of considering the off-diagonal noise, most of the non-Markovian computational methods only take the diagonal noise into account. Another nice feature of our setup is that, by design, we have a single-molecule setup which allows for detailed studies of non-Markovian energy transfer pathways.

An important feature of our proposal is the potential to achieve a high level of environment engineering, in such a way that external noise is used to benefit the quantum coherent energy transfer process inside the molecule. However, the broader scope of our work is along the lines of *biomimesis*: the artificial recreation of biological processes, which are already highly optimized through evolution.

Acknowledgments

The authors are indebted to S Ashhab, M Geller, F Nori, S Valleau, S Huelga and M H S Amin for valuable conversations. We acknowledge DARPA grant no. N66001-10-1-4060, NIST Award no. 60NANB10D267. This material is based upon work supported as a part of the Center for Excitonics, as an Energy Frontier Research Center funded by the US Department of Energy, Office of Science, Office of Basic Energy Sciences under Award no. DESC0001088. AE acknowledges financial support from the DFG under contract no. Ei 872/1-1. The work at MIT Lincoln Laboratory is sponsored by the United States Air Force under Air Force contract no. FA8721-05-C-0002. Opinions, interpretations, recommendations and conclusions are those of the authors and are not necessarily endorsed by the United States Government.

Appendix A. Figures and tables

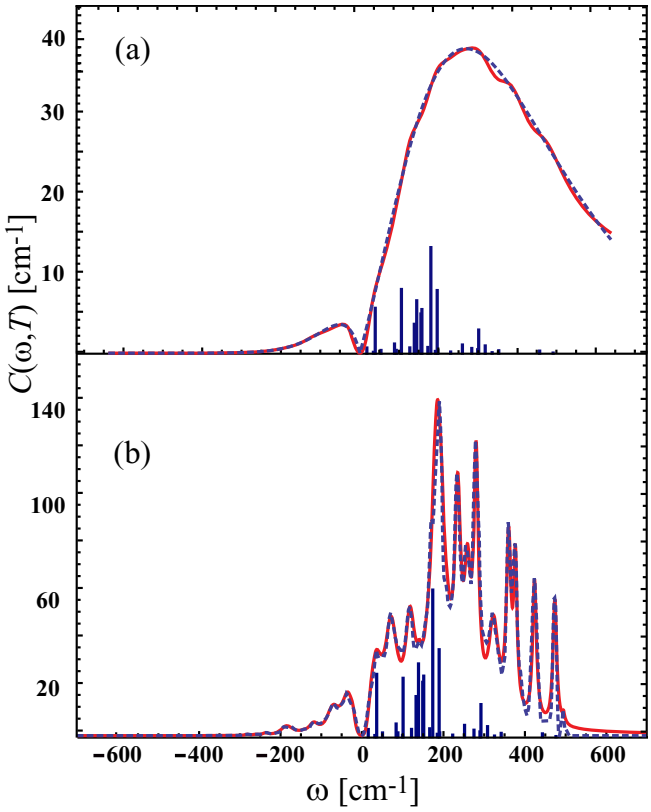

Figure A.1. The parameterization of the temperature-dependent (a) super-Ohmic SD and (b) experimental [38] SD of the FMO complex into distinct quantum oscillators. The blue dashed lines are the spectral densities and the red solid lines are accurate simulation with LRC oscillators coupled to the flux qubits, see figure 2(a). The temperature for both spectral densities is 77 K. The super-Ohmic SD is simulated with seven damped LRC oscillators and the experimental one is simulated with 15 damped oscillators. The blue bars show the transition energies [14] for the FMO complex.

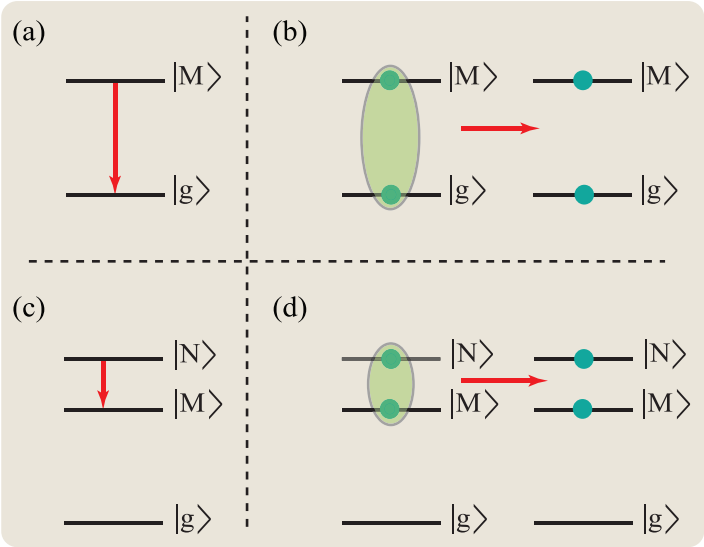

Figure A.2. Sketch of the basic processes in excitonic energy transfer. Consult table 1 (or table A.1) for numerical values of the time scales of the respective processes. Let $|g\rangle$ be the electronic ground state and $|M\rangle$ and $|N\rangle$ be two delocalized electronic excited states. (a) Decay between an excited state and the ground state, characterized with the *decay time* $\mathbb{T}_1$ (another name for this process is exciton recombination). (b) Dephasing of a superposition between ground state and an excited state. This process usually happens on a very fast time scale and is not relevant for the present discussion. (c) Decay in the single exciton manifold without the loss of the excitation to the ground state, characterized by the *decay time between exciton states*. (d) Dephasing in the single exciton manifold. Consider a superposition of exciton states $|\psi\rangle = \frac{1}{\sqrt{2}}(|M\rangle + |N\rangle)$. Then this dephasing process causes the initial density matrix $|\psi\rangle\langle\psi|$ to decay to an equal mixture $1/2(|M\rangle\langle M| + |N\rangle\langle N|)$ at long times. The time scale of this process is characterized by the *dephasing time in the single exciton manifold*.

Table A.1. Comparison of parameters for the FMO complex and the quantum simulator. The time scales shown below are for the dressed states of flux qubits coupled to the quantum harmonic oscillators. Notice that the decay time in a single qubit ($\mathbb{T}_1$) does not need to be mapped directly from the FMO dynamics. With nowadays achievable decay times in superconducting qubits, which are three orders of magnitude larger than the excitation transfer time between the qubits, the dynamics of the FMO complex can be simulated.

Parameter	FMO model	Quantum simulator
Decay time ($\mathbb{T}_1$) (single site electron–hole recombination)	$\approx$ ns	$\approx 10\,\mu$s
Average exciton transfer time (from site 8 to site 3)	≈ 5 ps	≈ 25 ns
Decay time between the exciton states (jump between exciton states)	$\approx$ ps	≈ 5 ns
Dephasing in exciton manifold (pure dephasing)	≈ 100 fs	≈ 500 ps
Time scale of quantum beatings (τ_{osc})	≈ 200 fs	≈ 1 ns
Coupling between sites	≈ 10–$122\,\text{cm}^{-1}$	≈ 60–730 MHz
Relative static site energy shifts $\lvert\tilde{\varepsilon}_i - \tilde{\varepsilon}_j\rvert \equiv \lvert\Delta_i - \Delta_j\rvert$	≈ 10–$500\,\text{cm}^{-1}$	≈ 60 MHz–3 GHz
Dynamic fast fluctuations [65] (dephasing rate)	$\approx 250 \pm 100\,\text{cm}^{-1}$ at 300 K	$\approx 1.5\,\text{GHz} \pm 600$ MHz
	$\approx 40 \pm 10\,\text{cm}^{-1}$ at 77 K	$\approx 240 \pm 60$ MHz
Temperature	300 K $\approx 208\,\text{cm}^{-1}$	60 mk ≈ 1.2 GHz
	100 K $\approx 69.5\,\text{cm}^{-1}$	20 mk ≈ 417 MHz
	77 K $\approx 53\,\text{cm}^{-1}$	15 mk ≈ 317 MHz

Table A.2. Decomposition of the temperature-dependent super-Ohmic spectral density at 300 K shown in figure 4(a) and simulation with six LRC oscillators coupled to each flux qubit, see figure 2(a).

	FMO complex		
	Transition frequency (cm^{-1})	Coupling strength (cm^{-1})	Quality factor
Oscillator no. 1	≈ 27	≈ 2.42	≈ 0.67
Oscillator no. 2	≈ 74	≈ 8.60	≈ 0.49
Oscillator no. 3	≈ 140	≈ 11.98	≈ 0.47
Oscillator no. 4	≈ 246	≈ 14.10	≈ 0.80
Oscillator no. 5	≈ 380	≈ 10.00	≈ 1.27
Oscillator no. 6	≈ 560	≈ 5.40	≈ 1.84
	Quantum simulator		
	Transition frequency	Coupling strength (MHz)	Quality factor
Oscillator no. 1	≈ 162 MHz	≈ 14.50	≈ 0.67
Oscillator no. 2	≈ 444 MHz	≈ 51.56	≈ 0.49
Oscillator no. 3	≈ 839 MHz	≈ 71.83	≈ 0.47
Oscillator no. 4	≈ 1.5 GHz	≈ 84.54	≈ 0.80
Oscillator no. 5	≈ 2 GHz	≈ 59.95	≈ 1.27
Oscillator no. 6	≈ 3 GHz	≈ 32.38	≈ 1.84

Table A.3. Decomposition of the temperature-dependent experimental [38] spectral density at 300 K shown in figure 4(b) and simulation with 15 LRC oscillators coupled to each flux qubit, see figure 2(a).

	FMO complex		
	Transition frequency (cm^{-1})	Coupling strength (cm^{-1})	Quality factor
Oscillator no. 1	≈ 20	≈ 3.0	≈ 0.93
Oscillator no. 2	≈ 37	≈ 5.9	≈ 1.35
Oscillator no. 3	≈ 72	≈ 9.7	≈ 1.89
Oscillator no. 4	≈ 118	≈ 7.8	≈ 4.00
Oscillator no. 5	≈ 142	≈ 2.8	≈ 9.00
Oscillator no. 6	≈ 190	≈ 16.5	≈ 5.00
Oscillator no. 7	≈ 237	≈ 10.4	≈ 8.80
Oscillator no. 8	≈ 260	≈ 6.1	≈ 10.80
Oscillator no. 9	≈ 282	≈ 9.9	≈ 11.75
Oscillator no. 10	≈ 325	≈ 4.8	≈ 18.06
Oscillator no. 11	≈ 363	≈ 6.3	≈ 20.17
Oscillator no. 12	≈ 380	≈ 5.3	≈ 29.23
Oscillator no. 13	≈ 426	≈ 4.4	≈ 30.43
Oscillator no. 14	≈ 478	≈ 3.4	≈ 48.00
Oscillator no. 15	≈ 500	≈ 1.3	≈ 35.71
	Quantum simulator		
	Transition frequency	Coupling strength (MHz)	Quality factor
Oscillator no. 1	≈ 120 MHz	≈ 18.00	≈ 0.93
Oscillator no. 2	≈ 222 MHz	≈ 35.38	≈ 1.35
Oscillator no. 3	≈ 432 MHz	≈ 58.16	≈ 1.89
Oscillator no. 4	≈ 707 MHz	≈ 46.77	≈ 4.00
Oscillator no. 5	≈ 851 MHz	≈ 16.79	≈ 9.00
Oscillator no. 6	≈ 1.1 GHz	≈ 98.93	≈ 5.00
Oscillator no. 7	≈ 1.4 GHz	≈ 62.36	≈ 8.80
Oscillator no. 8	≈ 1.6 GHz	≈ 36.57	≈ 10.80
Oscillator no. 9	≈ 1.7 GHz	≈ 59.36	≈ 11.75
Oscillator no. 10	≈ 1.9 GHz	≈ 28.78	≈ 18.06
Oscillator no. 11	≈ 2.2 GHz	≈ 37.77	≈ 20.17
Oscillator no. 12	≈ 2.3 GHz	≈ 31.79	≈ 29.23
Oscillator no. 13	≈ 2.6 GHz	≈ 26.38	≈ 30.43
Oscillator no. 14	≈ 2.9 GHz	≈ 20.39	≈ 48.00
Oscillator no. 15	≈ 3 GHz	≈ 7.79	≈ 35.71

Appendix B. Coordinate representation of the model Hamiltonian

In this section we derive the model Hamiltonian of a single molecule, given in equation (1) for $N = 1$, from the Born–Oppenheimer approximation. Restricting to two electronic states, the ground state $|g\rangle$ and the excited state $|e\rangle$, the Hamiltonian in the Born–Oppenheimer approximation is [30]:

$$H = H_{\mathrm{nuc,g}}(R)|g\rangle\langle g| + H_{\mathrm{nuc,e}}(R)|e\rangle\langle e|, \tag{B.1}$$

where R describes the collection of $3N_{\mathrm{nuc}}$ modes relevant to the molecule (both local and protein modes), $R = \{R_1, \ldots, R_{3N_{\mathrm{nuc}}}\}$, with N_{nuc} being the number of nuclei. The Hamiltonians $H_{\mathrm{nuc,g/e}}(R)$ describe the kinetic and potential energy of the nuclei, T_{nuc} and V_{nuc}, respectively: $H_{\mathrm{nuc,g/e}}(R) = T_{\mathrm{nuc}} + V_{\mathrm{nuc,g/e}}(R)$. The potential energy is given by $V_{\mathrm{nuc,g/e}}(R) = V_{\mathrm{nuc-nuc}}(R) + E_{\mathrm{g/e}}(R)$ with the inter-nuclear potential energy $V_{\mathrm{nuc-nuc}}$ and the potential energy due to the electrons $E_a(R)$. We assume a displaced harmonic oscillator model for the potential of ground and excited state:

$$V_{\mathrm{nuc,g}}(q) = U_{\mathrm{g}} + \sum_{i=1}^{3N_{\mathrm{nuc}}} \frac{\hbar\omega_i}{2} q_i^2, \tag{B.2}$$

$$V_{\mathrm{nuc,e}}(q) = U_{\mathrm{e}} + \sum_{i=1}^{3N_{\mathrm{nuc}}} \frac{\hbar\omega_i}{2} (q_i - d_i)^2. \tag{B.3}$$

Here, we introduced the renormalized coordinates $q = R - R_0$, where R_0 are the equilibrium positions in the electronic ground state (minimum of the ground state potential energy surface). The respective energies of the electronic states at the minimum of the respective potentials are U_{g} and U_{e}. We have assumed that the frequency ω_i of mode i remains unchanged in the exited state. The displacement of the ith mode in the excited state is given by d_i. The q-dependent energy gap is given by the difference of the two potentials:

$$V_{\mathrm{nuc,e}}(q) - V_{\mathrm{nuc,g}}(q) = \Delta U + \sum_{i=1}^{3N_{\mathrm{nuc}}} \frac{\hbar\omega_i}{2} d_i^2 - \sum_{i=1}^{3N_{\mathrm{nuc}}} \hbar\omega_i d_i q_i, \tag{B.4}$$

where the first term $\Delta U = U_{\mathrm{e}} - U_{\mathrm{g}}$ is the energy difference between the potential minima of ground and excited states. The second term gives the reorganization energy:

$$\lambda = \sum_i \lambda_i = \sum_i \frac{\hbar\omega_i}{2} d_i^2. \tag{B.5}$$

The third term gives the linear dependence of the gap on the coordinates of the harmonic oscillator, and is the exciton-vibrational coupling term. The total Hamiltonian in the harmonic approximation is thus:

$$H_{\mathrm{tot}} = \underbrace{\left(\Delta U + \sum_i \lambda_i\right) |e\rangle\langle e|}_{H_{\mathrm{el}}} + \underbrace{\left(T_{\mathrm{nuc}} + \sum_i \frac{\hbar\omega_i}{2} q_i^2\right) \mathbf{1}}_{H_{\mathrm{ph}}} + \underbrace{\sum_i \hbar\omega_i d_i q_i |e\rangle\langle e|}_{H_{\mathrm{el-ph}}}. \tag{B.6}$$

Here we defined the respective Hamiltonians for the electronic system, phonon bath and electron–phonon coupling, H_{el}, H_{ph} and $H_{\mathrm{el-ph}}$. The system identity operator is given by $1 = |g\rangle\langle g| + |e\rangle\langle e|$.

Appendix C. Energy transfer pathways for the FMO complex

We briefly explain the red arrows in figure 1(b), which show schematically the downwards energy transfer pathways for the FMO complex, similar to [63] which considered a seven-site model for the FMO complex.

From a system–bath model like equation (1), one can derive a master equation for the density matrix by using, for example, Redfield theory with the secular approximation [64]. Redfield theory assumes weak coupling and a Markovian bath. This leads to decoherence rates in the energy basis between energy states M and N given by [14] (without loss of generality $\hbar\omega_{MN} = E_M - E_N > 0$):

$$\Gamma^{\uparrow}_{MN} = 2\pi\ \gamma_{MN} J(\omega_{MN})\, n(\omega_{MN}), \tag{C.1}$$

$$\Gamma^{\downarrow}_{MN} = 2\pi\ \gamma_{MN} J(\omega_{MN})\, [n(\omega_{MN}) + 1]\,. \tag{C.2}$$

Here, $\Gamma^{\uparrow}_{MN}$ ($\Gamma^{\downarrow}_{MN}$) is the rate up (down) in energy and $n(\omega_{MN})$ is the mean number of vibrational quanta with energy $\hbar\omega_{MN}$ that are excited at a given temperature T:

$$n(\omega_{MN}) = 1/[\exp(\hbar\omega_{MN}/k_{\mathrm{B}}T) - 1]. \tag{C.3}$$

The factor $\gamma_{MN} = \sum_j |\langle M|j\rangle|^2 |\langle j|N\rangle|^2$ arises from the basis transformation between site and energy basis. In figure 1(a), the red arrows show a selected number of downward transitions with $\gamma_{MN} J(\omega_{MN}) \geqslant 0.3\,\mathrm{cm}^{-1}$.

References

[1] Kassal I, Whitfield J D, Perdomo-Ortiz A, Yung M-H and Aspuru-Guzik A 2011 *Annu. Rev. Phys. Chem.* **62** 185–207

[2] Feynman R P 1982 *Found. Phys.* **16** 507
Feynman R P 1986 *Int. J. Theor. Phys.* **21** 467

[3] Nielsen M A and Chuang I L 2000 *Quantum Computation and Quantum Information* (Cambridge: Cambridge University Press)

[4] DiVincenzo D P 2000 *Fortschr. Phys.* **48** 771–84 arXiv:quant-ph/0002077

[5] Buluta I and Nori F 2009 *Science* **326** 108–11

[6] Aspuru-Guzik A, Dutoi A D, Love P J and Head-Gordon M 2005 *Science* **309** 1704

[7] Schützhold R and Mostame S 2005 *JETP Lett.* **82** 248

[8] Mostame S and Schützhold R 2008 *Phys. Rev. Lett.* **101** 220501

[9] Tsomokos D I, Ashhab S and Nori F 2010 *Phys. Rev.* A **82** 052311

[10] Pritchett E J, Benjamin C, Galiautdinov A, Geller M R, Sornborger A T, Stancil P C and Martinis J M 2010 arXiv:1008.0701

[11] Engel G S, Calhoun T R, Read E L, Ahn T-K, Mancal T, Cheng Y-C, Blankenship R E and Fleming G R 2007 *Nature* **446** 782–6

[12] Lee H, Cheng Y-C and Fleming G R 2007 *Science* **316** 1462–5

[13] Cho M, Vaswani H M, Brixner T, Stenger J and Fleming G R 2005 *J. Phys. Chem.* B **109** 10542–56

[14] Adolphs J and Renger T 2006 *Biophys. J.* **91** 2778–97

[15] Müh F, Madjet M, El-A Adolphs J, Abdurahman A, Rabenstein B, Ishikita H, Knapp E-W and Renger T 2007 *Proc. Natl Acad. Sci.* **104** 16862–7

[16] Rebentrost P, Mohseni M, Kassal I, Lloyd S and Aspuru-Guzik A 2009 *New J. Phys.* **11** 033003

[17] Rebentrost P, Mohseni M and Aspuru-Guzik A 2009 *J. Phys. Chem.* B **113** 9942–7

[18] Caruso F, Chin A W, Datta A, Huelga S F and Plenio M B 2009 *J. Chem. Phys.* **131** 105106

[19] Palmieri B, Abramavicius D and Mukamel S 2009 *J. Chem. Phys.* **130** 204512

[20] Ishizaki A and Fleming G R 2009 *Proc. Natl Acad. Sci.* **106** 17255–60

[21] Sarovar M, Ishizaki A, Fleming G R and Whaley K B 2010 *Nature Phys.* **6** 462–7

[22] Rebentrost P and Aspuru-Guzik A 2011 *J. Chem. Phys.* **134** 101103

[23] am Busch M S, Müh F, Madjet M and El-A Renger T 2011 *J. Phys. Chem. Lett.* **2** 93–8

[24] Verstraete F, Wolf M M and Cirac J I 2009 *Nature Phys.* **5** 633–6

[25] Barreiro J T *et al* 2011 *Nature* **470** 486–91
[26] Yu L-B *et al* 2010 arXiv:1012.5764
[27] Niskanen A O, Harrabi K, Yoshihara F, Nakamura Y, Lloyd S and Tsai J S 2007 *Science* **316** 723–6
[28] Hime T, Reichardt P A, Plourde B L T, Robertson T L, Wu C-E, Ustinov V and Clarke J 2006 *Science* **314** 1427–9
[29] Fowler A G, Thompson W F, Yan Z, Stephens A M, Plourde B L T and Wilhelm F K 2007 *Phys. Rev.* B **76** 174507
[30] May V and Kühn O 2004 *Charge and Energy Transfer Dynamics in Molecular Systems* (Weinheim: Wiley-VCH)
[31] Olbrich C, Strümpfer J, Schulten K and Kleinekathöfer U 2011 *J. Phys. Chem.* B **115** 758–64
[32] Shim S, Rebentrost P, Valleau S and Aspuru-Guzik A 2012 *Biophys. J.* **102** 649–60
[33] Valleau S, Eisfeld A and Aspuru-Guzik A 2012 Reason is but choosing: On the different alternatives for bath correlators and spectral densities from mixed quantum-classical simulations arXiv:1207.3087
[34] Leggett A J, Chakravarty S, Dorsey A T, Fisher M P A, Garg A and Zwerger W 1987 *Rev. Mod. Phys.* **59** 1–85
[35] Egorov S A, Everitt K F and Skinner J L 1999 *J. Phys. Chem.* A **103** 9494–9
[36] Ritschel G, Roden J, Strunz W T and Eisfeld A 2011 *New J. Phys.* **13** 113034
[37] Haken H and Reineker P 1972 *Z. Phys.* **249** 253–68
Haken H and Strobl G 1973 *Z. Phys.* **262** 135–48
[38] Wendling M, Pullerits T, Przyjalgowski M A, Vulto S I E, Aartsma T J, van Grondelle R and van Amerongen H 2000 *J. Phys. Chem.* B **104** 5825–31
[39] Seibt J, Winkler T, Renziehausen K, Dehm V, Würthner F, Meyer H-D and Engel V 2009 *J. Phys. Chem.* A **113** 13475–82
[40] Strümpfer J and Schulten K 2009 *J. Chem. Phys.* **131** 225101
[41] Kreisbeck C, Kramer T, Rodríguez M and Hein B 2011 *J. Chem. Theory Comput.* **7** 2166
[42] Kreisbeck C and Kramer T 2012 arXiv:1203.1485
[43] Clarke J and Wilhelm F K 2008 *Nature* **453** 1031–42
[44] Yoshihara F, Harrabi K, Niskanen A O, Nakamura Y and Tsai J S 2006 *Phys. Rev. Lett.* **97** 167001
[45] Ashhab S, Niskanen A O, Harrabi K, Nakamura Y, Picot T, de Groot P C, Harmans C J P M, Mooij J E and Nori F 2008 *Phys. Rev.* B **77** 014510
[46] Paauw F G, Fedorov A, Harmans C J P M and Mooij J E 2009 *Phys. Rev. Lett.* **102** 090501
[47] Chiorescu I, Nakamura Y, Harmans C J P M and Mooij J E 2003 *Science* **299** 1869–71
[48] Omelyanchouk A N, Savel'ev S, Zagoskin A M, Il'ichev E and Nori F 2009 *Phys. Rev.* B **80** 212503
[49] Semiao F L, Furuya K and Milburn G J 2010 *New J. Phys.* **12** 083033
[50] Caruso F, Spagnolo N, Vitelli C, Sciarrino F and Plenio M B 2011 *Phys. Rev.* A **83** 013811
[51] Eisfeld A and Briggs J S 2012 *Phys. Rev.* E **85** 046118
[52] Hauss J, Fedorov A, Hutter C, Shnirman A and Schön G 2008 *Phys. Rev. Lett.* **100** 037003
[53] Bertet P, Chiorescu I, Burkard G, Semba K, Harmans C J P M, DiVincenzo D P and Mooij J E 2005 *Phys. Rev. Lett.* **95** 257002
[54] Bertet P, Chiorescu I, Harmans C J P M and Mooij J E 2005 arXiv:cond-mat/0507290
[55] Steffen M, Kumar S, DiVincenzo D P, Rozen J R, Keefe G A, Rothwell M B and Ketchen M B 2010 *Phys. Rev. Lett.* **105** 100502
[56] Mori H 1965 *Prog. Theor. Phys.* **34** 399–416
[57] Hughes K H, Christ C D and Burghardt I 2009 *J. Chem. Phys.* **131** 024109
[58] Prior J, Chin A W, Huelga S F and Plenio M B 2010 *Phys. Rev. Lett.* **105** 050404
[59] Reed M D, DiCarlo L, Nigg S E, Sun L, Frunzio L, Girvin S M and Schoelkopf R J 2012 *Nature* **482** 382–385
[60] Lucero E, Barends R, Chen Y, Kelly J, Mariantoni M, Megrant A, O'Malley P, Sank D, Vainsencher A, Wenner J, White T, Yin Y, Cleland A N and Martinis J M 2012 *Nature Physics*, doi:10.1038/nphys2385, arXiv:1202.5707

[61] Kerman A J and Oliver W D 2008 *Phys. Rev. Lett.* **101** 070501
[62] Kerman A J 2010 *Phys. Rev. Lett.* **104** 027002
[63] Brixner T, Stenger J, Vaswani H M, Cho M, Blankenship R E and Fleming G R 2005 *Nature* **434** 625–8
[64] Breuer H P and Petruccione F 2002 *The Theory of Open Quantum Systems* (New York: Oxford University Press)
[65] Panitchayangkoon G, Hayes D, Fransted K A, Caram J R, Harel E, Wen J, Blankenship R E and Engel G S 2010 *Proc. Natl Acad. Sci.* **107** 16862–7